CRYSTAL GROWTH & DESIGN

Article

pubs.acs.org/crystal

Controllable Assembly of Al-MIL-100 via an Inducing Occupied Effect and Its Selective Adsorption Activity

Mo Qiu,[§] Qingxin Guan,[§] and Wei Li*[,§,†]

[§]College of Chemistry, Key Laboratory of Advanced Energy Materials Chemistry (Ministry of Education) and [†]Collaborative Innovation Center of Chemical Science and Engineering (Tianjin), Nankai University, Tianjin, 300071, China

Supporting Information

ABSTRACT: This work reports a novel method to selectively synthesize framework isomer MOF crystals. Al-MIL-100 and Al-MIL-96 are framework isomers and could be obtained purposefully by adding an inducing agent using a microwave irradiation method. The inducing agent has an occupying effect by a PO_4 tetrahedron group, which favors the formation of basic building units of Al-MIL-100. Spontaneously, zeolite $AlPO_4$ or SAPO-34 was employed as an inducing agent for rapid and controllable synthesis of single phase Al-MIL-100. The results show that the gradual releasing of phosphate from the solid surface during the early stage of synthesis plays a crucial role in the occupying action. Subsequently, a possible growth mechanism of Al-MIL-100 is proposed. Finally, the resulting Al-MIL-100 exhibits a nice stability and a remarkable selective adsorption ability for N-heterocyclic molecules from fuels.

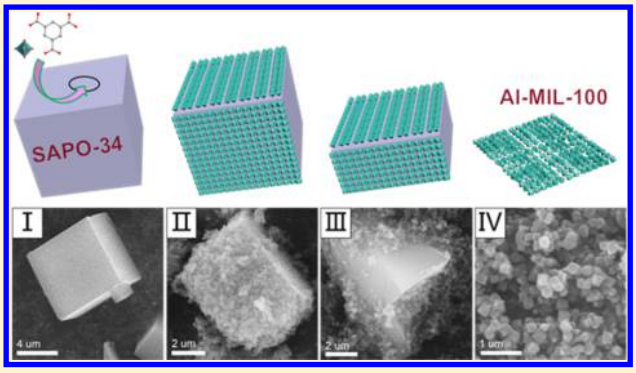

1. INTRODUCTION

Metal−organic frameworks (MOFs), a kind of porous crystal material, are composed of metal ions connected with organic ligands by self-assembly. In the past several decades, much research of MOFs has been focused on the design of novel frameworks, the functionality of the structures, and the development of applications and properties.[1−6] However, the synthesis of MOFs still is a complicated and time-consuming process. How to rapidly and selectively synthesize single-phase MOFs is challenging research.

According to previously published papers, there are two pathways to synthesize MOFs rapidly. One is using a nonsolvothermal synthesis method, such as microwave irradiation, or ultrasonic methods.[7−9] MOFs could be synthesized in a few minutes using these methods, which is equivalent to the efficiency of solvent thermal methods of several days. Another method is to introduce crystal seeds into the synthesis system to accelerate the crystallization of MOFs. It is reported that using a heterogeneous nucleus to accelerate formation of MOFs can alter the kinetics of MOFs' crystallization.[10] Falcaro et al. showed that α-hopeite microparticles could be used as a nucleation seed to promote the framework growth of MOF-5.[11] Compared with the conventional solvothermal synthesis, this heterogeneous nucleation improved the synthesis efficiency by about 70%. Subsequently, the modified nanosized SiO_2 particles was used as the crystallization nucleating agent of MOF-5 to economize the reaction time significantly.[12] Zhang and co-workers have used zeolite mordenite (MOR) crystal seeds for the rapid hydrothermal synthesis of Cr-MIL-101. This method could shorten the crystallization time by 75% compared with conventional MIL-101 crystallization, making it possible for rapid production of MOFs on a larger scale.[13]

However, the controllable synthesis of MOFs is also essential, but more difficult to achieve, especially for those polymorphs.[14,15] Recently, Xu and co-workers reported a facile seed-mediated approach to synthesize a target phase-pure MOF. The particular Zr-MOF was used as the seeds, the nucleation stage was bypass, and the approach can also be applied to other MOFs.[16] Zou et al. have reported that three vanadium MILs (V-MIL-88B, V-MIL-101, and V-MIL-47) which have the same SBU were obtained selectively by changing the synthesis conditions.[17] Similarly, Al-MIL-96[18] and Al-MIL-100[19] are also topological framework isomers with the same basic building units which linked together in different spatial arrangements. Therefore, a mixed-phase product was apt to be generated in the crystallization process. Compared with Al-MIL-96, Al-MIL-100 has a wider application field owing to the larger specific surface areas and more Lewis acid sites.[18,19] The method of synthesis of Al-MIL-100 is diverse. Xia et al. have reported a method to facilely synthesize MIL-100(Al) based gels through a supercritical CO_2 drying process.[20] To obtain a pure phase of Al-MIL-100, Férey and co-workers utilized Me_3btc as a ligand to slow down the hydrolysis process of H_3btc then control the synthetic process.[19] According to these results, Li's group[21] adopted a way of later entry of

Received: January 21, 2016
Revised: May 16, 2016
Published: June 9, 2016

DOI: 10.1021/acs.cgd.6b00103
Cryst. Growth Des. 2016, 16, 3639−3646

methyl or ethyl groups to synthesize pure phase Al-MIL-100 with H_3btc directly. After the pH value of the solution was regulated by HNO_3, the target products of pure phase Al-MIL-100 were obtained in the DMF aqueous solution. This method opened up a new field in the synthesis of MOF with additional groups. However, a simple method of synthesizing Al-MIL-100 was desired. Férey and co-workers have used in situ NMR to reveal the essential difference between Al-MIL-100 and Al-MIL-96 during crystallization.[22] As shown in Figure 1, one Al_2-$(btc)_2$ dimer can be combined with two aluminum monomers to form the building unit of MIL-96. Differently, one Al_2-$(btc)_2$ dimer combined with one aluminum monomer to form the building unit of MIL-100. On the basis of the above results, we assumed the addition of a synthetic inducing agent, containing some kind of specific group to form a particular chemical bonding, which could occupy the position denoted α instead of aluminum monomer. The occupying action could control the coordination number of the aluminum monomer, thus controling the synthesis of MIL-100. The inducing agent must possess two features. One is the occupying action, and the other is that the occupying group can be slowly released in the synthesis system to avoid competitive coordination with reactants. For this purpose, the PO_4 tetrahedron unit in zeolites was selected. On the one hand, hydrogen bonding interaction could occur between PO_4 tetrahedron and H_3btc,; on the other hand, the PO_4 tetrahedron in zeolites could gradually be obtained under the reaction condition of synthesis (pH value is about 2).

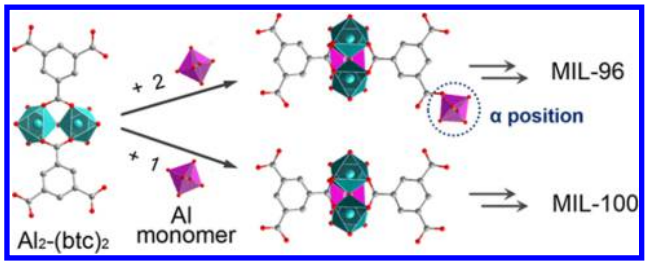

Figure 1. Schematic illustration for the formation of Al-MIL-96 and Al-MIL-100 crystals integrate units.

Herein, $AlPO_4$ and/or SAPO-34 was employed as an inducing agent for rapid and controllable synthesizing single phase Al-MIL-100. Subsequently, a possible growth mechanism for of Al-MIL-100 was proposed. Finally, adsorption ability of Al-MIL-100 was tested using N/S-heterocyclic molecules.

2. EXPERIMENTAL SECTION

Materials. SAPO-34, SAPO-11, ZSM-5, MCM-41, and SBA-15 were purchased from Tianjin Chemist Scientific Ltd.; other reagents were analytical pure grade and purchased from Alfa Aesar.

Synthesis of $AlPO_4$. The synthesis of $AlPO_4$ is illustrated as follows 3.75 g of $Al(NO_3)_3{\cdot}9H_2O$ and 1.32 g of $(NH_4)_2HPO_4$ were dissolved in 30 mL of deionized water under stirring with a mole ratio of Al:P = 1:1. After stirring for 1 h, the solution was evaporated slowly to dehydrate and was dried at 130 °C for 5 h to obtain the precursor. Finally, the white precursor was treated at 550 °C for 1 h in air to obtain $AlPO_4$.

Synthesis of NiPO and CoPO. The NiPO and CoPO were prepared by the same method as for $AlPO_4$, with $Al(NO_3)_3{\cdot}9H_2O$ substituted by $Ni(NO_3)_2{\cdot}6H_2O$ or $Co(NO_3)_2{\cdot}6H_2O$, respectively.

Synthesis of Al-MIL-100. A total of 0.460 g of $Al(NO_3)_3{\cdot}9H_2O$ (1.22 mmol) and 0.210 g of H_3btc (1.00 mmol) were added to a 35 mL quartz vessel containing 7 mL of distilled water. Subsequently the required amount of inducing agent was added, and the mixture was stirred for 5 min; the pH value of the solution was 2.1. Then the vessel was sealed and placed in a microwave reactor (Discover, CEM, maximum power 300 W). The instrument operated at a power of 150 W and autogenic pressure up to 300 psi. Then the vessel was heated from room temperature to 190 °C within 5 min, and this temperature was maintained for a certain period of time. After the mixture was cooled to room temperature, the white solid was isolated by centrifugation and washed with DMF and ethanol three times. Then the products were dried in a vacuum oven at 120 °C for 3 h (inducing-agents including: $AlPO_4$, SAPO-34, SAPO-11, NiPO, CoPO).

Synthesis of Al-MIL-96. Compared with Al-MIL-100, Al-MIL-96 was obtained by the same method as mentioned above, but without adding any inducing agents to the synthesis solution. The sample was post processed as described for Al-MIL-100.

Materials Characterization. Powder X-ray diffraction patterns (XRD) of samples were obtained on a Bruker D8 focus diffractometer, with Cu Kα radiation at 40 kV and 40 mA. The sizes and morphologies of samples were examined using a scanning electron microscope (SEM, JEOL, JSM-7500F) with EDX analysis, and transmission electron microscope (TEM, Philips Tecnai G^2 F-20). Nitrogen adsorption−desorption isotherms of samples were measured at 77 K on a BELSORP-Mini instrument. Before measurement, the samples were evacuated at 423 K for 6 h. The surface area was calculated using a multipoint Brunauer−Emmett−Teller (BET) model. The Fourier transform infrared (FTIR) spectra of the samples before and after adsorption were recorded on a Nicolet Nexus 470 FTIR Spectrometric Analyzer using KBr pellets. The thermal stability of the samples was measured by a NETZSCH TG 290 analyzer in air at a heating rate of 10 °C min^{-1} up to 800 °C. The concentrations of quinolone/*n*-heptane solution were analyzed with an Agilent 7890A GC equipped with a flame ionization detector and an INNOWAX column.

Adsorption Test. The batch adsorption experiments were carried out at 293 K in a 50 mL flask in a temperature-controlled water bath. In a standard procedure, the Al-MIL-100 materials were pretreated at 423 K in an oven for 10 h under atmospheric conditions before adsorption. Then, Al-MIL-100 (0.03 g) was added to *n*-Heptane solution with a certain concentration of nitrogen or sulfur compounds. Uptakes were calculated directly from gas chromatography (GC) output data.

The adsorption amount (q_e) of quinoline was calculated according to the following equation:

$$q_e = \frac{V(C_0 - C_e)}{m}100\% \quad (1)$$

3. RESULTS AND DISCUSSION

Characterization Results. Two porous aluminum trimesates, MIL-96 and MIL-100, were assembled from the same components, but have distinct crystallographic structures. However, a pure phase of aluminum trimesates was difficult to synthesize with H_3btc as ligand in the published papers because of the phase conversion between MIL-100 and MIL-96. Our previous work has investigated the phase transition of aluminum trimesates with the synthesis time under MW irradiation. The XRD patterns of the products are shown in Figure S1. Compared with the stand simulated XRD patterns, the typical diffraction peak at $2\theta = 9.1°$ is attributed to MIL-96; the diffraction peaks of MIL-100 are detected at 2θ = 2.1, 3.4, 4.0, and 10.4°.[18,19] MW irradiation leads to the synthesis of MIL-100 along with a small amount of MIL-96 at 10 min, and a pure phase of Al-MIL-96 when the reaction time was increased to 30 min. MIL-100 was first synthesized and subsequently converted into MIL-96 with increasing reaction time. The latest research findings suggest MIL-100 is kinetically controlled phase, whereas MIL-96 is the thermodynamically controlled

DOI: 10.1021/acs.cgd.6b00103
Cryst. Growth Des. 2016, 16, 3639−3646

phase.[22−24] During the synthesis, it would be a dynamic process of precursor species for crystallization and recrystallization, which leads to the mixed phases.[25]

For the purpose of verifying our proposed idea of inducing synthesis and eliminating the interference of other groups, homogeneous metal-containing $AlPO_4$ was prepared and used as an inducing agent in the above synthesis process. The XRD results of products induced by 0.01 and 0.05 g of $AlPO_4$ are shown in Figure 2 (irradiation time were 30 min). The XRD

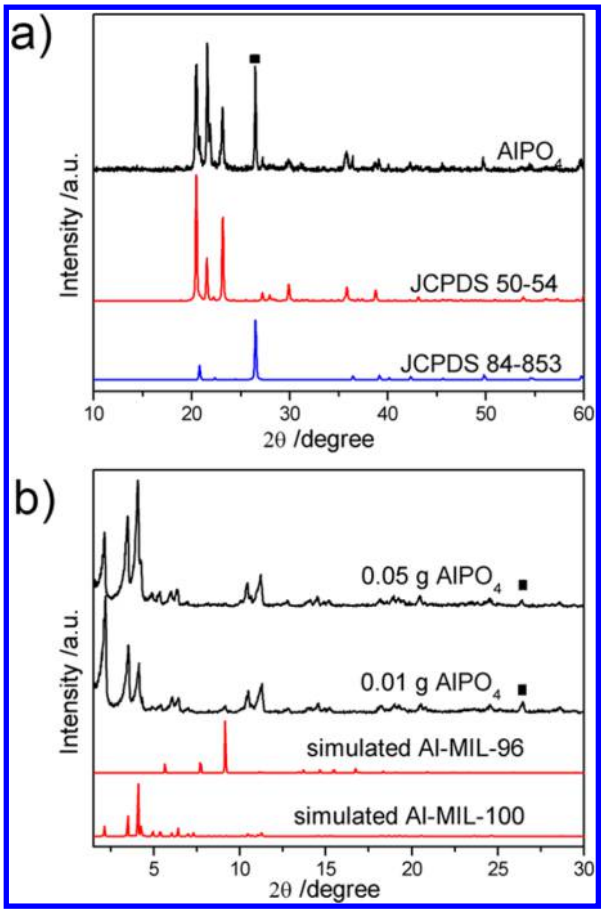

Figure 2. XRD patterns of (a) $AlPO_4$ and (b) as-prepared Al-MIL-100 induced by $AlPO_4$.

peaks of the product match well with the pure phase of Al-MIL-100; just 26.4° is indexed to the characteristic peak of $AlPO_4$ (Figure 2b), indicating that $AlPO_4$ is capable of induced synthesizing Al-MIL-100 by gradually releasing PO_4 tetrahedron groups. Nanosized octahedral products were observed in the SEM images, which were the same as Al-MIL-100 reported in the literature (Figure S2).[19,22]

For rapidly controllable synthesis of Al-MIL-100, SAPO-34 was also used as an inducing agent, which is a class of silicon aluminum phosphate zeolites.[26] It will be decomposed in a high-temperature acidic solution (pH = 2) of the synthesis system under MW irradiation. The Al−O bond would break first; the resulting PO_4 tetrahedron group would have the occupational ability in synthesizing Al-MIL-100. The characterization results of as-prepared MIL-100 (irradiation time was 10 min, 0.01 g of SAPO-34 was added) are shown in Figure 3 and 4. The results show that the XRD patterns of as-prepared Al-MIL-100 matched well with the pure phase Al-MIL-100. In addition, there are no characteristic diffraction peaks of SAPO-

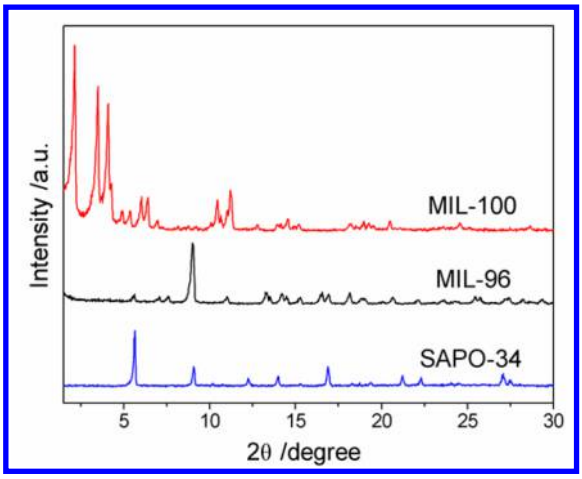

Figure 3. XRD patterns of Al-MIL-100 (induced by SAPO-34), Al-MIL-96 and SAPO-34.

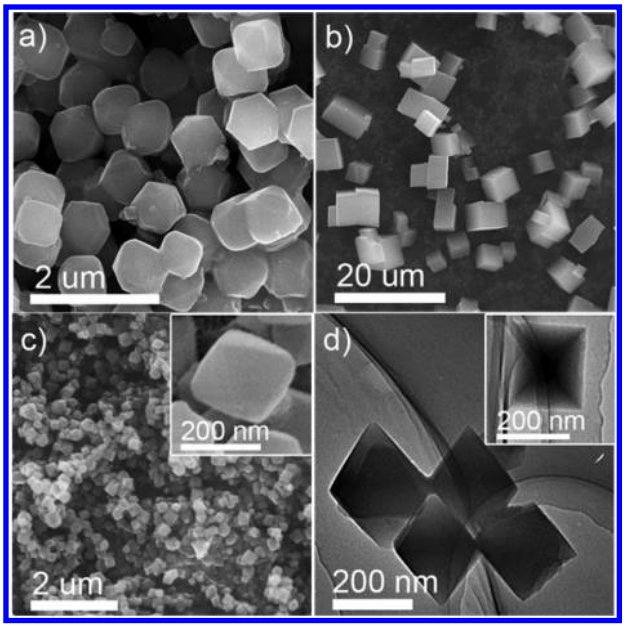

Figure 4. SEM images of Al-MIL-96 (a), SAPO-34 (b) and Al-MIL-100 (c). TEM images of Al-MIL-100 (d).

34 or MIL-96 in the XRD patterns of as-prepared Al-MIL-100, indicating that the product was a single phase Al-MIL-100. Figure 4a displays a pure phase MIL-96 has a polyhedral morphology with a size of about 1 μm. The morphology of SAPO-34 zeolite is a cube with a size of 10−20 μm (Figure 4b). Figure 4c,d is typical SEM and TEM images of as-prepared MIL-100. The product is a nearly uniform monodisperse octahedron with a size of about 200−400 nm. Similarly, no SAPO-34 and Al-MIL-96 are observed in the SEM or TEM images of as-prepared MIL-100, also indicating that a single phase product was obtained.

The results of XRD and SEM show that no SAPO-34 were detected in the product. One possible reason is that SAPO-34 had been involved in the reaction and was exhausted. Another is that the additional amount of SAPO-34 was too few that below the detection limit. Hence, usage amount of SAPO-34 was investigated, and the corresponding XRD patterns are shown in Figure S3a. The results indicate that SAPO-34 was fully, and the obtained products were single phase Al-MIL-100.

DOI: 10.1021/acs.cgd.6b00103
Cryst. Growth Des. 2016, 16, 3639−3646

The XRD results show that the MIL-96 did not appear with reaction time increasing (Figure S3b).

The properties and thermal stability of Al-MIL-100 (irradiation time was 10 min, 0.01 g SAPO-34 was added) were shown in Figure S4a. The surface area of the sample is 1576 m^2/g, which is similar to the literature.[19] The TG curve of Al-MIL-100 is shown in Figure S4b, and the Al-MIL-100 sample exhibits a high thermal stability (410 °C) and has three processes of weight loss, consistent with the previous reports.[19]

In order to evaluate the existing form and occupation mechanism of SAPO-34 in the synthesis of Al-MIL-100, in Figure 5a, the spectra of SAPO-34 exhibit prominent peaks at

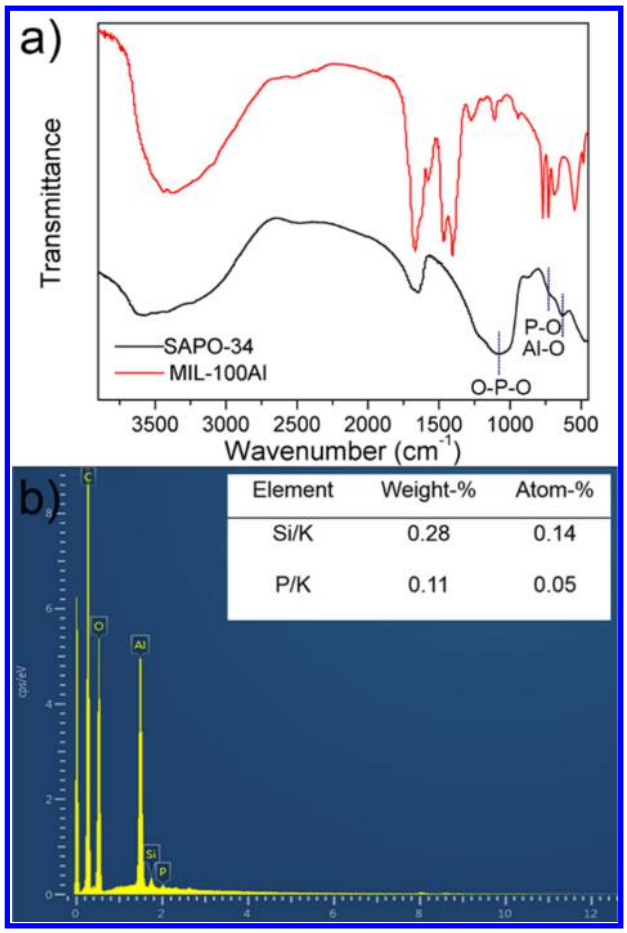

Figure 5. (a) FTIR spectra of SAPO-34 and as-prepared Al-MIL-100 and (b) EDX pattern of as-prepared Al-MIL-100 (irradiation time was 10 min, 0.01 g of SAPO-34 was added).

628, 772, and 1074 cm^{-1}. The peak at 628 cm^{-1} is attributed to a double six-member ring vibration of the SAPO-34 framework, 772 cm^{-1} belongs to a symmetric vibration of the P−O or Al−O bond and 1074 cm^{-1} is an asymmetric vibration peak of O−P−O.[12] However, these characteristic peaks were not found in the FTIR spectra of product Al-MIL-100, which indicates that SAPO-34 was not involved in the framework of product. Moreover, the FTIR spectra of product is in accordance with that of the Al-MIL-100 synthesized by the conventional method.[19] In addition, the EDS results were shown in Figure 5b. The results indicate that Si was presented in the product with a very small amount, whereas the content of P is close to the error range. It can be concluded that, after the decomposition of SAPO-34, SiO_2 was difficult to remove and did not participate in the inducing process. Differently, the PO_4 tetrahedron not only provided an occupying effect, but also can be removed in the subsequent washing steps.

Mechanism Analysis. SAPO-34 exhibited the occupation effect on the synthesis of Al-MIL-100 as we expected. For comparison, ZSM-5, MCM-41, and SBA-15 were also used in the induced synthesis of Al-MIL-100. The XRD and SEM results were shown in Figures S5−S7. Mixed-phase products were obtained for the three zeolites in the synthesis system. ZSM-5, MCM-41, and SBA-15 did not have the property of inducing synthesis. Compared with SAPO-34, they had no occupying groups after decomposition under the synthesis condition. Therefore, the phosphorus-containing group is the key factor in inducing synthesis, which should be slowly released during decomposition to avoid competition coordination with reactants. To prove this point of view, we have selected Na_3PO_4 as an inducing agent to add to the synthesis process. The results in Figure S8a indicate that the PO_4^{3-} group obtained by fast dissolution of Na_3PO_4 did not possess the ability of occupying effect to obtain the single-phase MIL-100. Meanwhile, PO_4^{3-} did not have the occupation effect due to PO_4^{3-} of Na_3PO_4 was fully dissolved in water to affect the coordination number with H_3btc. Therefore, PO_4 tetrahedron played the role of occupation rather than PO_4^{3-} group.

The occupying process of the PO_4 tetrahedron was also illustrated in Figure S9. For comparison, Na_2HPO_4 and NaH_2PO_4 were selected to add to the synthesis solution. The results in Figure S8b,c show that PO_4 tetrahedron really played the role of occupying action, and the existing form of phosphorus after the MW reaction should be $H_2PO_4^-$.

As we mentioned above, MIL-96 and MIL-100 are two porous aluminum trimesate isomers, which are crystallized from identical reactants, but with different spatial arrangements. Férey et al. have investigated the real synthesis process of the two isomers and have demonstrated that they are definitely different from their chromium or iron analogues, which exhibit the trimeric oxo unit as the dominant species in the synthesis solution.[22] No trimer unit is detected in the synthesis solution of MIL-100 and MIL-96, and each phase could be formed from Al_2-$(btc)_2$ and Al monomer in solution (Figure 1). The two complexes played an important role in the formation of crystals. The process is as follows: the first step is the formation of Al_2-$(btc)_2$ and Al monomer in solution, and further aggregated to form units as a result of a supersaturated solution. Then, the units condensed to a connected network, and finally the network transformed into a periodic framework. Therefore, controlling the connection way of Al_2-$(btc)_2$ and Al monomer is vital to control the phase of the crystals.

According to our experimental results and the structural analysis of Al-MIL-96 and Al-MIL-100, a possible mechanism for the induced synthesis of Al-MIL-100 by SAPO-34 zeolite was proposed. As shown in Figure 6, the PO_4 groups and a carboxyl of Al-$(btc)_1$ would form Al-$(btc)_1$-PO_4 through hydrogen-bond interaction. Subsequently, Al_2-$(btc)_2$-$(PO_4)_2$ dimer is formed by the combination of two of Al-$(btc)_1$-PO_4. Then, the Al_2-$(btc)_2$-$(PO_4)_2$ dimer can be combined with one aluminum monomer to form the building unit (Al_3-$(btc)_2$-$(PO_4)_2$) of MIL-100, owing to the occupying ability of PO_4 tetrahedron group. The primary structure of Al-MIL-100 unit (super tetrahedron) were gradually generated by three such units ($Al_3O(H_2O)_2(OH)(btc)_2$) after automatically removing the PO_4 groups during combination. Because of the occupying role of PO_4 tetrahedron group in the process, the position of

DOI: 10.1021/acs.cgd.6b00103
Cryst. Growth Des. 2016, 16, 3639−3646

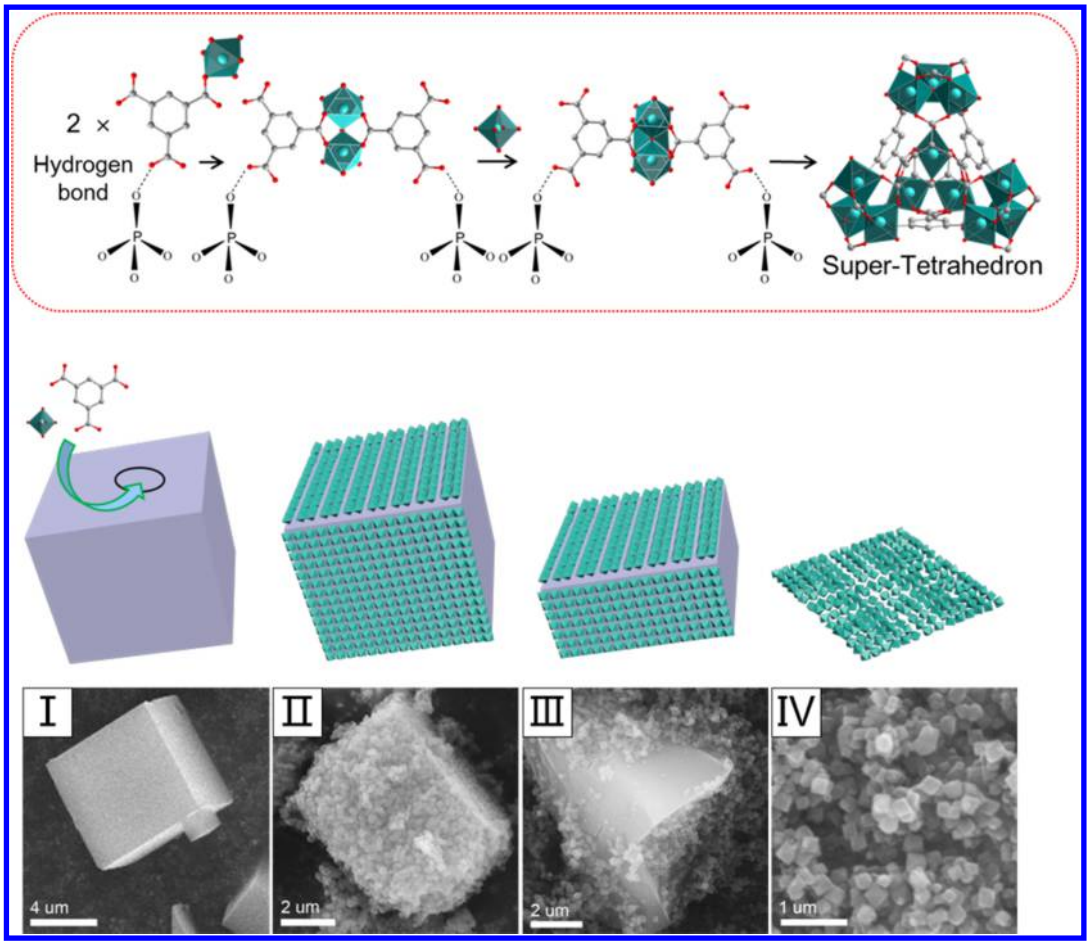

Figure 6. Mechanism of induced synthesis: schematic illustration of the formation of basic unit of Al-MIL-100, Al-MIL-100 crystal, and SEM images of the synthesis process.

the other Al monomer was occupied, which can hinder the formation of Al-MIL-96. The supertetrahedron would continue to form two cages and finally generate the crystal structure of Al-MIL-100.

The gradual decomposition and consuming processes of SAPO-34 are schematically indicated in Figure 6. As shown in Figure 6, SAPO-34 was decomposed gradually with the consumption of PO_4 tetrahedron groups, and subsequently the as-prepared Al-MIL-100 would depart from SAPO-34. Finally, SAPO-34 was exhausted entirely and Al-MIL-100 was obtained in solution. The SEM images of the process corresponding with the model diagram are shown in Figure 6. SAPO-34 with microsize crystals is exhausted by generating nanoscale Al-MIL-100 crystals. Consequently, the process of Al-MIL-100 crystal formation is induced by the SAPO-34, and the inducing activity can be attributed to an occupational effect.

To further verify the formation mechanism of Al-MIL-100, SAPO-11 was also investigated. The results in Figure S10 illustrate that the products are all Al-MIL-100 and also unaffected by the dosage of SAPO-11. The results imply that SAPO-11 also possessed the ability to induce synthesis by gradually releasing PO_4 tetrahedron groups in the synthesis process.

Similarly, to further demonstrate the proposed mechanism, we attempted to extend this method to heterogeneous metal-containing additives, which were obtained by self-made and denoted as NiPO and CoPO (irradiation time were 10 min). As shown in Figure 7a, the XRD pattern of the product induced by 0.01 g of NiPO is consistent with the pattern of Al-MIL-100 induced by SAPO-34, only with a slight change in the main peak intensity. However, the pattern was no longer attributed to Al-MIL-100 when induced by 0.05 g of NiPO, and the SEM images (induced by 0.01 g of NiPO are shown in Figure S11a,b) indicated that the as-prepared products are also nanosized octahedra with no inducing-agent observed. The XRD (Figure 7b) and SEM (Figure S11c,d) results for CoPO as inducing agent are the same as for NiPO. These results revealing that NiPO or CoPO could gradually releasing PO_4 group to induce the formation of Al-MIL-100. When adding an excess amount, the heterogeneous metal Ni or Co would coordinate with ligands by competing with Al. The BET curves of the two products induced by NiPO and CoPO are given in Figure 7c. The BET specific surface areas of them are 1550 and 1534 m^2/g, respectively. The TG results (Figure 7d) show that the stability of the two products is similar to the product of inducing by SAPO-34. Moreover, the curves have lost more qualities (water molecules) in the first and second weight loss stages, which shows that the products induced by NiPO and CoPO may have a better adsorption ability of water. Similar results were also reported by Jeremias; Al-MIL-100 could be the adsorbent for water.[27] As for the location of the heterogeneous metal in the frameworks, the EDX results (Figure S12) illustrated that the amount of Ni or Co is close to the margin of error.

Adsorption Performance of Different Adsorbates. Selective adsorption is a significant separation method for N/

DOI: 10.1021/acs.cgd.6b00103
Cryst. Growth Des. 2016, 16, 3639−3646

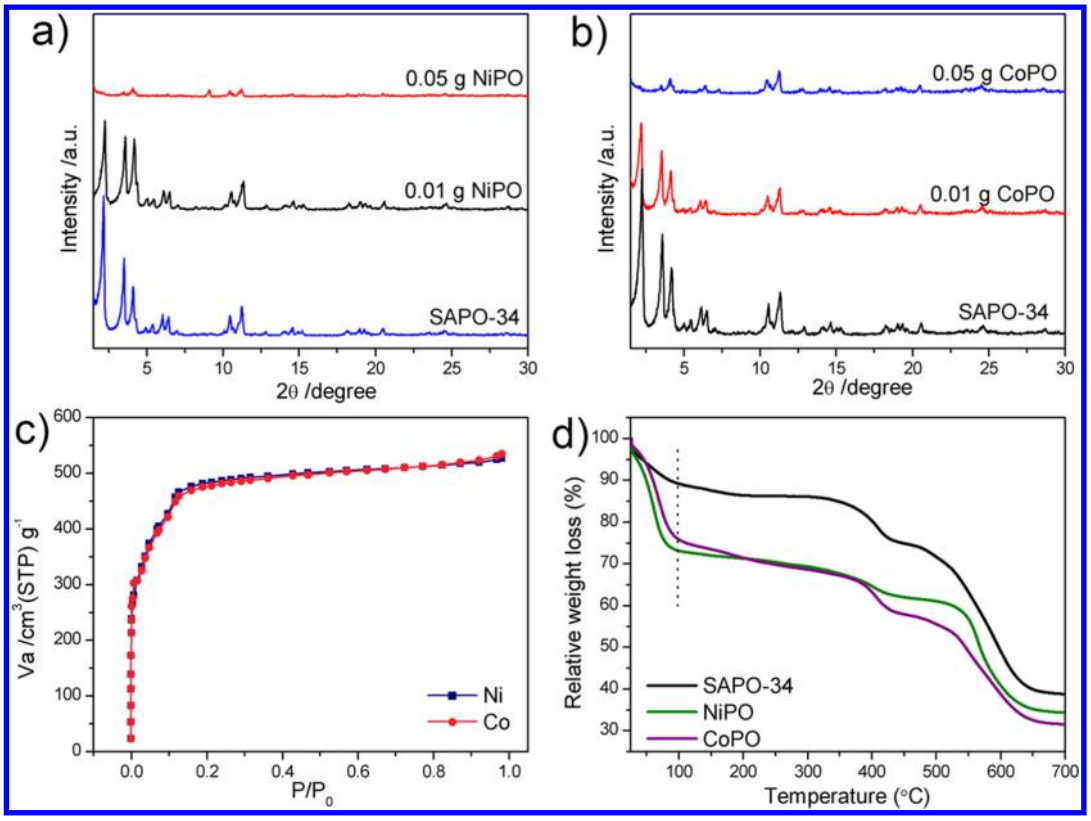

Figure 7. XRD patterns of the product induced by (a) NiPO and (b) CoPO as induced agent. (c) Nitrogen adsorption isotherm and (d) TG curve of the product induced by NiPO and CoPO.

S heterocyclic molecules in fuel. Hence, a large number of adsorbents with selective ability have been designed to separate N/S heterocyclic molecules, especially for N heterocyclic molecules.[28,29] In this regard, Jhung's group did much valuable work in adsorptive desulfurization and denitrogenation with MOFs. We could obtain an understanding of the current state of ADS and AND.[30] Vokringer and his co-workers have investigated the acid sites of Al-MIL-100 by infrared spectroscopy, for its potential application in adsorption and catalysis.[31]The Al-MIL-100 products induced by SAPO-34 (irradiation time was 10 min, 0.01 g of SAPO-34 was added) have been investigated to remove N/S heterocyclic molecules by adsorption from simulated fuel. N-Heptane was employed as a solvent to dissolve the relevant organic molecules. The adsorption was investigated under the same initial concentration (2 mmol/L) using the same dose of Al-MIL-100 (0.03 g) adsorbent at 293 K. Figure 8a shows that the adsorption abilities of Al-MIL-100 for these heterocyclic compounds are quite different. According to the result of the column chart, MIL-100 exhibits a high adsorption ability for nitrogen-containing heterocyclics in fuel. The amount of equilibrium adsorption of pyridine is up to 1.38 mmol/g, and the amount of quinoline is up to 1.09 mmol/g. However, only 0.16 mmol/g of thiophene was removed over MIL-100 under the same conditions. This result is associated with previously published papers.[28] The adsorption amounts of organic molecules with nitro and amino on a benzene ring was lower than the amounts of pyridine and quinoline owing to the steric effect. Therefore, the ensuing discussion focuses on the adsorption of quinoline to obtain a better understanding of the removal of quinoline by adsorption.

Adsorption Kinetics. According to the published paper, weight based units were used.[32,33] Adsorption was carried at different initial concentrations (200, 400, 600, and 800 mg/L). The quinoline uptake rate and the contact time of the adsorption were described with adsorption kinetics at 293 K. As the results show in Figure 8b, all of the apparent adsorption equilibriums were usually established within 30 min, showing a rapid adsorption of quinoline onto Al-MIL-100. The adsorption curves maintained the same trend with different initial concentration. Pseudo-first-order and pseudo-second-order kinetic model were used to fit the results. The results are in Figure S13 and Table 1 and 2, respectively. And indicating that the pseudo-second-order kinetic model is more suitable to describe the adsorption kinetics of quinoline onto Al-MIL-100. The experimental results follow the pseudo-second-order kinetic equation.

Reused and Adsorption Mechanism. The reusability of Al-MIL-100 was demonstrated from the recycling experiments of adsorption of quinoline with an initial concentration of 800 mg/L at 293 K. As shown in Figure 9a, after three cycles of adsorption, the adsorbents retained 80% capacity when used for the second time and only 55% for the fourth use. The reason for this might be some structural damage to Al-MIL-100 caused by acid washing. Because the synthesis solution was an acid condition (pH = 2.0) and the as-prepared Al-MIL-100 was stable in the acid solution for a few days, we have chosen the diluted acid (1 M HNO_3) washing for 1 h to regenerate the adsorbent. The reused experiments were performed before filtering and drying. Moreover, it could be concluded that quinoline molecular adsorption onto Al-MIL-100 is a chemisorption. The XRD patterns (Figure S14a) for the reused adsorbent indicate that the MOF's structure was completely

DOI: 10.1021/acs.cgd.6b00103
Cryst. Growth Des. 2016, 16, 3639−3646

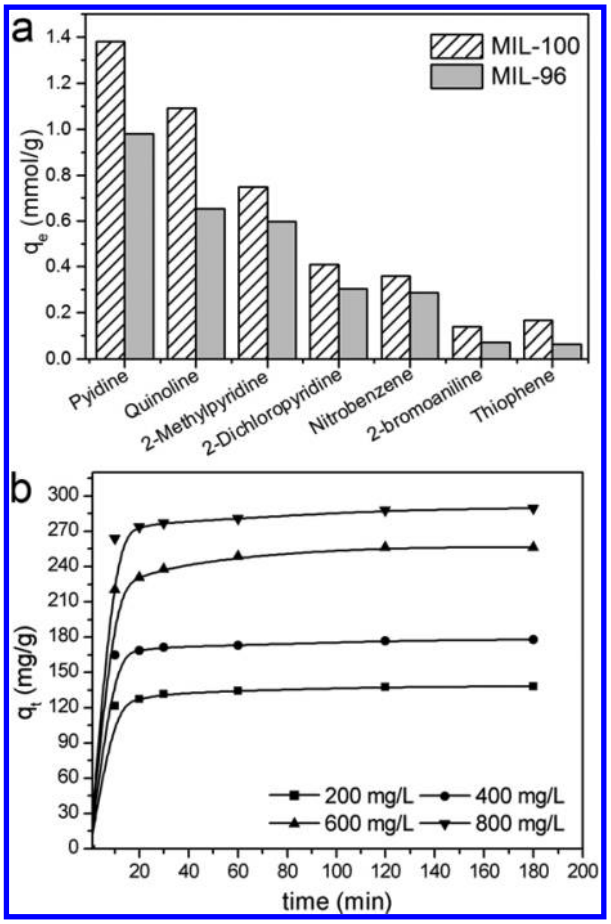

Figure 8. (a) Adsorption amounts of different organic compounds onto Al-MIL-100 and Al-MIL-96 and (b) adsorption curves of different initial concentrations of quinoline onto Al-MIL-100 (T = 293 K).

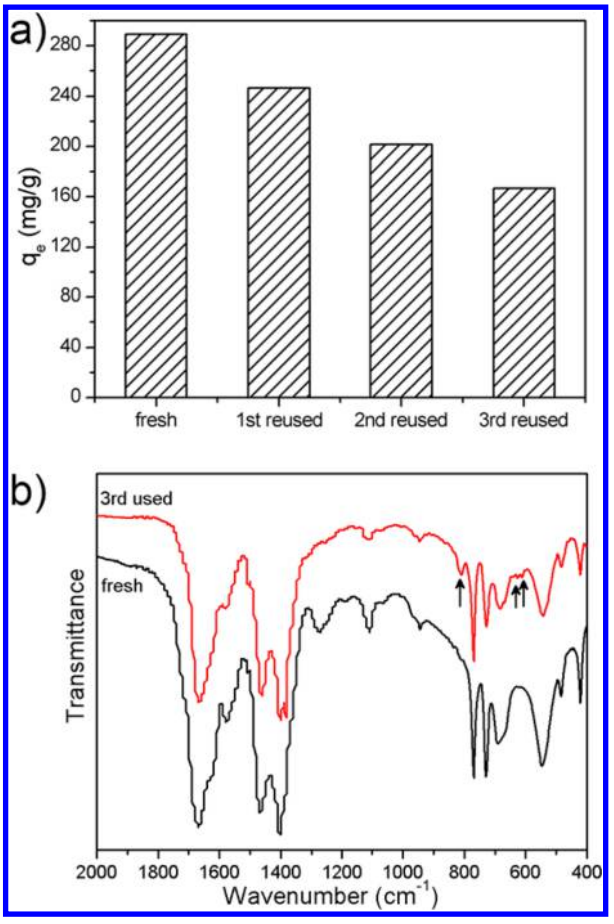

Figure 9. (a) The reused of Al-MIL-100 on adsorption of quinoline (concentration 800 mg/L, T = 293 K) and (b) FT-IR spectra of fresh and recycle for three times of Al-MIL-100.

Table 1. Pseudo-First-Order Kinetics Constants of Quinoline Adsorption on MIL-100

concentration (mg/L)	K_1 (min^{-1})	$q_{e,cal}$ (mg/g)	R^2	$q_{e,exp}$ (mg/g)
200	2.63×10^{-2}	56	0.582	139
400	2.56×10^{-2}	50	0.521	178
600	3.23×10^{-2}	137	0.632	256
800	2.34×10^{-2}	214	0.866	289

Table 2. Pseudo-Second-Order Kinetics Constants of Quinoline Adsorption on MIL-100

concentration (mg/L)	K_2 (g/mg min)	$q_{e,cal}$ (mg/g)	R^2	$q_{e,exp}$ (mg/g)
200	5.33×10^{-3}	140	1.000	139
400	6.05×10^{-3}	178	1.000	178
600	2.30×10^{-3}	258	1.000	256
800	2.26×10^{-3}	291	1.000	289

preserved after adsorption, only with the degree of crystallinity decreasing. The SEM image of the adsorbent after three repeated adsorptions is almost unchanged compared with fresh samples (Figure S14b).

The structure of Al-MIL-100 is a three-dimensional framework, building up from the supertetrahedral (ST) blocks. The ST block is composed of trinuclear aluminum octahedral units (Figure S14a) connecting to each other through the ligands to form two types of cavities: denoted as S and L. This primary structural unit $Al_3O(H_2O)_2(OH)$ $(btc)_3$ is the focus of our discussion. The terminal Al−O bond of the oxygen sharing μ_3-oxo-bridging structure has a bond length of 1.894−2.005 Å). Two H_2O molecules and a hydroxyl OH were needed to balance the framework charges. Each oxygen atom would typically hydrogen bond with H_2O molecules within S/L cages to generate Lewis acid sites to provide sufficient adsorption sites.[19] Moreover, when a polar molecule with a lone pair of electrons interacts with MIL-100, it would occupy the open position generated by activating the pores of Al-MIL-100.

The nitrogen atom of quinoline has three SP2 hybrid orbitals and a lone pair of electrons, generating the weak alkalinity of quinoline. In the process of adsorption, the alkaline quinoline molecular would interact with the Lewis acid sites of Al-MIL-100 (purple balls) to form a stronger coordinated bond than Al−O(H_2O/OH) with the Al atom. As a result, the position of water molecules or hydroxyl groups was substituted by the nitrogen atom of quinoline. The formation of the coordinated bond can also be explained with FTIR spectra. As shown in Figure 9b, it was reported that the small peaks at 625 and 609 cm^{-1} and the infrared absorption peak at 814 cm^{-1}, could be attributed to the characteristic vibration absorption peaks of the quinoline ring.[34] This illustrates that a stronger coordinated bond was formed between quinoline and Al atom, which could not be destroyed after washing. Therefore, Al-MIL-100 could selectively adsorb nitrogenous heterocyclic in fuel.

DOI: 10.1021/acs.cgd.6b00103
Cryst. Growth Des. 2016, 16, 3639−3646

4. CONCLUSIONS

In summary, we have reported a method for the rapid and selective synthesis of Al-MIL-100 crystals by microwave irradiation in 10 min. Zeolite was used as inducing agent in phase-selective synthesis of MOFs for the first time. Comprehensive characterization of the products indicated that the as-prepared Al-MIL-100 was single phase, and the gradual releasing PO_4 tetrahedron group of SAPO-34 in solution was the key factor of the occupational ability. It favors the formation of MIL-100 SBU and shows a remarkable tendency to nucleate MIL-100 crystals through the occupying effect. Other inducing-agents were also added to the synthesis process, which have demonstrated the validity of the mechanism. The as-prepared Al-MIL-100 is stable and exhibits highly selective adsorption activity on N-heterocyclic molecules especially quinoline in fuel, due to the Lewis acid sites in the framework. In conclusion, the strategy of employing occupied groups by synthetic inducing-agent in this paper is visualized to open a new way for fabricating MOFs with control.

■ ASSOCIATED CONTENT

Supporting Information

The Supporting Information is available free of charge on the ACS Publications website at DOI: 10.1021/acs.cgd.6b00103.

XRD patterns of different synthesis time with and without an inducing agent; SEM images of $AlPO_4$ and Al-MIL-100 induced by $AlPO_4$; different dosage of SAPO-34 and different reaction times; the nitrogen adsorption isotherm and TG curve of the prepared Al-MIL-100; the XRD patterns and SEM images of different inducing agents (ZSM-5, MCM-41, and SBA-15) and their induced products; the XRD patterns of different phosphates as inducing agent (Na_3PO_4, Na_2HPO_4, and NaH_2PO_4); the schematic illustration of the occupying process of the PO4 tetrahedron; the XRD patterns and SEM images of SAPO-11 as the inducing agent; the SEM images and EDX patterns of the products induced by NiPO and CoPO; the kinetics plots of quinoline adsorbed onto Al-MIL-100 at different initial concentrations in 293 K; the Lagergren pseudo-first-order kinetic model and the Ho−Mckay pseudo-second-order rate model; the XRD patterns and SEM images of reused adsorbents; the models build of SBU of Al-MIL-100 (PDF)

■ AUTHOR INFORMATION

Corresponding Author

*Phone/Fax: 86-22-23508662. E-mail: weili@nankai.edu.cn.

Notes

The authors declare no competing financial interest.

■ ACKNOWLEDGMENTS

This work was financially supported by the NSFC (21376123, U1403293), MOE (IRT-13R30 and 113016A), and the Research Fund for 111 Project (B12015).

■ REFERENCES

(1) Burtch, N. C.; Jasuja, H.; Walton, K. S. *Chem. Rev.* **2014**, *114*, 10575−10612.
(2) Jiang, J.; Yaghi, O. M. *Chem. Rev.* **2015**, *115*, 6966−6997.
(3) Zhao, D.; Timmons, D. J.; Yuan, D.; Zhou, H. C. *Acc. Chem. Res.* **2011**, *44*, 123−133.
(4) Luan, Y.; Qi, Y.; Gao, H.; Zheng, N.; Wang, G. *J. Mater. Chem. A* **2014**, *2*, 20588−20596.
(5) Morris, W.; Briley, W. E.; Auyeung, E.; Cabezas, M. D.; Mirkin, C. A. *J. Am. Chem. Soc.* **2014**, *136*, 7261−7264.
(6) Dhakshinamoorthy, A.; Garcia, H. *Chem. Soc. Rev.* **2014**, *43*, 5750−5765.
(7) Khan, N. A.; Jhung, S. H. *Coord. Chem. Rev.* **2015**, *285*, 11−23.
(8) Zheng, N.; Masel, R. I. *J. Am. Chem. Soc.* **2006**, *128*, 12394−12395.
(9) Jung, D.-W.; Yang, D.-A.; Kim, J.; Kim, J.; Ahn, W.-S. *Dalton Trans.* **2010**, *39*, 2883−2887.
(10) Doherty, C. M.; Buso, D.; Hill, A. J.; Furukawa, S.; Kitagawa, S.; Falcaro, P. *Acc. Chem. Res.* **2014**, *47* (2), 396−405.
(11) Buso, D.; Hill, A. J.; Colson, T.; Whitfield, H. J.; Patelli, A.; Scopece, P.; Doherty, C. M.; Falcaro, P. *Cryst. Growth Des.* **2011**, *11* (12), 5268−5274.
(12) Falcaro, P.; Hill, A. J.; Nairn, K. M.; Jasieniak, J.; Mardel, J. I.; Bastow, T. J.; Mayo, S. C.; Gimona, M.; Gomez, D.; Whitfield, H. J.; Riccò, R.; Patelli, A.; Marmiroli, B.; Amenitsch, H.; Colson, T.; Villanova, L.; Buso, D. *Nat. Commun.* **2011**, *2*, 237.
(13) Liu, S.; Zhang, Y.; Meng, Y.; Gao, F.; Jiao, S.; Ke, Y. *Cryst. Growth Des.* **2013**, *13*, 2697−2702.
(14) Makal, T. A.; Yakovenko, A. A.; Zhou, H. C. *J. Phys. Chem. Lett.* **2011**, *2*, 1682−1689.
(15) Zhang, J.-P.; Huang, X.-C.; Chen, X.-M. *Chem. Soc. Rev.* **2009**, *38*, 2385−2396.
(16) Xu, H.-Q.; Wang, K.; Ding, M.; Feng, D.; Jiang, H.-L.; Zhou, H. − C. *J. Am. Chem. Soc.* **2016**, *138*, 5316−5320.
(17) Carson, F.; Su, J.; Platero-Prats, A. E.; Wan, W.; Yun, Y.; Samain, L.; Zou, X. *Cryst. Growth Des.* **2013**, *13*, 5036−5044.
(18) Loiseau, T.; Lecroq, L.; Volkringer, C.; Marrot, J.; Férey, G.; Haouas, M.; Taulelle, F.; Bourrelly, S.; Llewellyn, P. L.; Latroche, M. *J. Am. Chem. Soc.* **2006**, *128*, 10223−10230.
(19) Volkringer, C.; Popov, D.; Loiseau, T.; Férey, G. R.; Burghammer, M.; Riekel, C.; Haouas, M.; Taulelle, F. *Chem. Mater.* **2009**, *21*, 5695−5697.
(20) Xia, W.; Zhang, X.; Xu, L.; Wang, Y.; Lin, J.; Zou, R. *RSC Adv.* **2013**, *3*, 11007−11013.
(21) Yang, J. F.; Wang, J.; Deng, S. G.; Li, J. P. *Chem. Commun.* **2016**, *52*, 725−728.
(22) Haouas, M.; Volkringer, C.; Loiseau, T.; Férey, G.; Taulelle, F. *Chem. Mater.* **2012**, *24*, 2462−2471.
(23) Khan, N. A.; Lee, J. S.; Jeon, J.; Jun, C.-H.; Jhung, S. H. *Microporous Mesoporous Mater.* **2012**, *152*, 235−239.
(24) Sindoro, M.; Jee, A.-Y.; Granick, S. *Chem. Commun.* **2013**, *49*, 9576−9578.
(25) Lin, Y.; Kong, C.; Chen, L. *Chem. - Asian J.* **2013**, *8*, 1873−1878.
(26) Iwase, Y.; Motokura, K.; Koyama, T. R.; Miyaji, A.; Baba, T. *Phys. Chem. Chem. Phys.* **2009**, *11*, 9268−9277.
(27) Jeremias, F.; Khutia, A.; Henninger, S. K.; Janiak, C. *J. Mater. Chem.* **2012**, *22*, 10148−10151.
(28) Van de Voorde, B.; Boulhout, M.; Vermoortele, F.; Horcajada, P.; Cunha, D.; Lee, J. S.; Chang, J.-S.; Gibson, E.; Daturi, M.; Lavalley, J.-C.; Vimont, A.; Beurroies, I.; De Vos, D. E. *J. Am. Chem. Soc.* **2013**, *135*, 9849−9856.
(29) Maes, M.; Trekels, M.; Boulhout, M.; Schouteden, S.; Vermoortele, F.; Alaerts, L.; Heurtaux, D.; Seo, Y.-K.; Hwang, Y. K.; Chang, J.-S.; Beurroies, I.; Denoyel, R.; Temst, K.; Vantomme, A.; Horcajada, P.; Serre, C.; De Vos, D. E. *Angew. Chem., Int. Ed.* **2011**, *50*, 4210−4214.
(30) Ahmed, I.; Jhung, S. H. *J. Hazard. Mater.* **2016**, *138*, 5316−5320.
(31) Volkringer, C.; Leclerc, H.; Lavalley, J.-C.; Loiseau, T.; Férey, G.; Daturi, M.; Vimont, A. *J. Phys. Chem. C* **2012**, *116*, 5710−5719.
(32) Chen, C.; Zhang, M.; Guan, Q.; Li, W. *Chem. Eng. J.* **2012**, *183*, 60−67.
(33) Huo, S.-H.; Yan, X.-P. *J. Mater. Chem.* **2012**, *22*, 7449−7455.
(34) Dines, T. J.; MacGregor, L. D.; Rochester, C. H. *Langmuir* **2002**, *18*, 2300−2308.

DOI: 10.1021/acs.cgd.6b00103
Cryst. Growth Des. 2016, 16, 3639−3646